Detailed Modeling of a Novel Photovoltaic Thermal Cascade Heat Pump Domestic Water Heating System

J. P. Fine, J. Friedman, and S. B. Dworkin*

Mechanical and Industrial Engineering, Ryerson University

350 Victoria Street, Toronto, Canada

(*Corresponding author: seth.dworkin@ryerson.ca)

Abstract

A domestic water heating system that combines photovoltaic thermal (PVT) solar collectors with two heat pumps, in a novel cascade arrangement, is presented and analyzed in this paper. The goal of this analysis is to determine and compare the annual thermal energy output of the PVT cascade heat pump system with an evacuated tube and simultaneous consumption PVT single heat pump water heating system. The computational technique that was developed to analyze the PVT cascade heat pump system, which determines solar panel energy outputs, and heat pump operating characteristics, is described in detail. Case study simulation results are also presented, which include transient power output profiles, temperature profiles, and yearly energy output results. Hourly weather data, including air dry-bulb temperatures and solar flux values, from locations with a range of climates was used in these simulations. The results of this study show that the PVT cascade heat pump system has an annual thermal energy output improvement over the evacuated tube heating system ranging from 37% to 68%, depending on the selected simulation location.

Keywords: PVT; Solar; Domestic hot water; Heat Pump; Hybrid; Renewable

1 Introduction

The use of solar energy for water heating is becoming more popular as the cost of solar collectors fall and concerns over GHG emissions increase around the world. However, most solar water heating systems still require an auxiliary heat source since the temperature of the fluid emerging from the solar collector may not meet the required hot water supply temperature

[1, 2, 3]. Alternatively, if a system is set up such that the outlet temperature of the fluid from the collector is constrained to be sufficient for hot water production, the system will operate with lower thermal efficiency.

Along with investigations into using solar energy for domestic hot water production, there are also several ongoing studies investigating the use of heat pump systems for domestic water heating. However, in cold climates, the coefficient of performance of these heat pump systems are diminished because of the large temperature differences between the evaporating and condensing heat exchangers in these systems [4, 5]. Therefore, a novel solution to low system efficiencies is discussed in this paper.

This novel solution implements a hybrid photovoltaic thermal (PVT) collector, coupled with two heat pump loops, which are in a cascade arrangement. The electrical energy generated by the solar collector is used to power the compressors in both of the heat pumps, and the heat pumps upgrade the temperature of the thermal energy generated by the solar collector, along with a secondary low quality heat source

First, a review of existing studies into solar collector heat pump systems will be presented in Section 2. In Sections 3 and 4, the PVT cascade heat pump system, and the analysis technique developed to analyze this system, will be presented. Finally, the results of a comparative case study between a conventional solar water heating system and the PVT heat pump system will be presented in Section 5.

2 Heat Pump Solar Collecting System Review

An investigation into existing methods for coupling heat pumps with solar collectors was carried out at the beginning of this study. Four different methods were identified during this

literature review, which are photovoltaic powered heat pumps, solar assisted heat pumps, separate consumption PVT heat pumps, and simultaneous consumption PVT heat pumps. These methods will be discussed below.

2.1 Photovoltaic Powered Heat Pumps

The first method involves powering the compressor in a heat pump cycle with a PV panel [6, 7]. These systems do not utilize the waste heat generated on the solar collector, and only use the solar collector as an electrical energy source. A study carried out by Izquierdo et al. [6] used a PV panel to charge a battery, which then powered a compressor in a heat pump cycle. One drawback to this system is that there is wasted thermal energy generated by the PV panel, which not only could be harnessed, but also causes the temperature of the PV panel to rise, resulting in lower PV electrical energy outputs [8]. Another drawback of this system is the inefficiency associated with charging and discharging the system's battery [9]. Overall, a heat output equal to 18% of the incident solar irradiation was realized at the condenser in this system [6].

2.2 Solar Assisted Heat Pump

The second method involves the use of a solar thermal collector as a thermal energy source for a heat pump cycle [7, 10, 11]. These systems can use the solar thermal collector as the primary thermal energy source, or as a secondary thermal energy source. This system type does not include PV cells, and therefore the electrical power supplied to the compressor must be provided by an external source. A reduction in external electrical energy consumption of 12% can be realized when using this system type for domestic hot water production [10].

2.3 Separate Consumption PVT Heat Pump

The third method involves the use of a PVT panel, but the heat pump cycle only utilizes the thermal energy from the panel, while the electrical energy generated by the panel is consumed by an external system, and the electricity that powers the compressor is provided from another external system [8, 12, 13, 14]. These systems attempt to optimize both the thermal and electrical energy outputs of the PVT panel, but these energy streams are consumed by separate systems. These systems can operate with refrigerant flowing through the PVT panel, which results in the PVT panel acting as the evaporator in the heat pump cycle. Alternatively, a non-evaporating working fluid can be passed through the PVT panel, and the refrigerant in the heat pump can be evaporated in a second heat exchanger. The research being carried out on these systems is concerned with optimization of the detailed mechanical design of the PVT panel, such that optimal thermal and electrical energy extraction can occur [8, 12, 13, 14]. Finally, studies show that 40-60% of the total solar energy incident on the solar collector can be used with this system arrangement [13].

2.4 Simultaneous Consumption PVT Heat Pump

The fourth method involves using a PVT panel to provide both thermal energy and electrical energy to a heat pump cycle [15,16,17]. The system being investigated by Zhang et al. [15] couples a heat pump with an array of PVT panels, and the compressor in the heat pump is powered directly from the array's generated electricity. The electrical energy consumption of the heat pump compressor is entirely dependent on the useful thermal energy produced by the PVT panel, along with the selected working fluid states in the heat pump loop. In cases where all available thermal energy from the panel is extracted, and excess electrical energy remains, Zhang

et al. anticipate that the excess electricity will be sold to the grid, or stored in a battery [15]. The main drawback of this system, compared to the three previously mentioned methods, is its complexity. Another drawback is that in systems where the excess electricity cannot be used externally, it would be wasted. However, Zhang et al. have shown that this system has environmental and economic benefits, and can produce a heat output equal to 50% of the incident solar irradiation at its condenser [16, 17].

The design discussed in this paper builds on the simultaneous consumption PVT heat pump system proposed by Zhang et al. by adding a secondary heat pump loop. The use of two heat pump loops is a novel system arrangement, and allows for system parameter optimization to maximize thermal energy output [18]. The feasibility of this system is supported by the common and successful implementation of cascade heat pumps in industry [4], along with the successful implementation of the simultaneous consumption PVT heat pump system by Zhang et al. [15].

3 PVT Cascade Heat Pump System Design

The PVT cascade heat pump system in this study uses both the heat and electrical energy generated by the PVT panel in the heat pump. However, unlike the PVT heat pump system mentioned in Section 2.4, the system in this paper contains a secondary heat pump loop. The addition of a secondary heat pump loop allows for all of the electrical energy generated by the PVT panel to be usefully consumed within the system, instead of wasting energy, relying on a battery for electrical energy storage, or relying on a grid connection for energy sale [18]. A schematic of the PVT cascade heat pump system is shown in Figure 1.

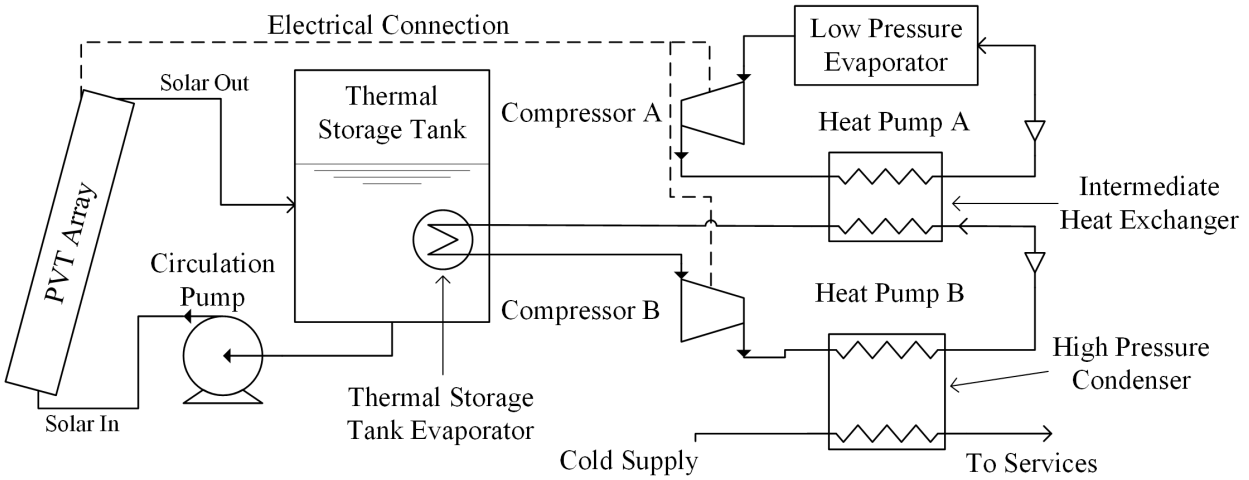

Figure 1: PVT Heat Pump System with Component Labels

A coolant fluid is circulated through the PVT array, which extracts thermal energy and adds it to the thermal storage tank. The coolant is assumed to circulate only when the thermal efficiency of the array is greater than zero, and it operates using an on/off control scheme. Therefore, the flowrate through the panel is either zero, or a constant value that is determined based on manufacture guidelines. The thermal energy that is injected into the thermal storage tank then causes the temperature of the tank to increase, while the mass of fluid within the tank is kept constant.

A heat pump loop (heat pump B) evaporator contained within the thermal storage tank is used to extract heat from the thermal storage tank. This evaporator is assumed to be maintained at a constant pressure, and therefore its evaporation temperature can be taken as constant. It follows that heat can only be removed from the thermal storage tank when the temperature of the tank is sufficiently above this constant evaporator temperature, which is defined as the minimum thermal storage tank temperature. When the thermal storage tank is below this minimum temperature, the heat pump loops are deemed inoperable.

At times when the thermal storage tank is at or above the minimum temperature, the heat pump loops become operational. The compressors in each heat pump loop are assumed to be powered directly from the electrical energy generated by the PVT array. Heat pump loop B is given priority to consume this electrical energy, which results in scenarios where only loop B is operating if there is not enough electricity to also power loop A. However, at times when there is sufficient electrical power for both heat pump loops, then heat is taken from another low temperature heat source through a low pressure evaporator. This heat source can be the ambient environment, a geo-exchange loop, or any other freely available low-grade heat source.

The heat from heat pump loop A is passed into heat pump loop B through the intermediate heat exchanger, which acts as the condenser for loop A and an evaporator for loop B. This heat, along with the heat from the thermal storage tank, passes though heat pump loop B, and is then used to heat water for domestic purposes at the condenser in loop B.

Since variable speed compressors are used in both heat pump loops, the mass flow rates of refrigerant in each heat pump loop are assumed to be variable, and are proportional to the electrical energy supplied to each heat pump loop's compressor. The mass flow rate of the cold supply water through the high pressure condenser in heat pump loop B is assumed to be sufficient to maintain thermal equilibrium within the system, based on the selected refrigerant states. Finally, the refrigerant used in the heat pump loops can be the same, or different, and would be selected based on the conditions in which the system will operate.

4 Analysis Technique

The analysis of the PVT heat pump system was carried out using a time-stepping method. System equilibrium and constant system parameters were assumed during each time-step in the

analysis. The schematic shown in Figure 2 includes labelled state locations, which will be used in the proceeding analysis description.

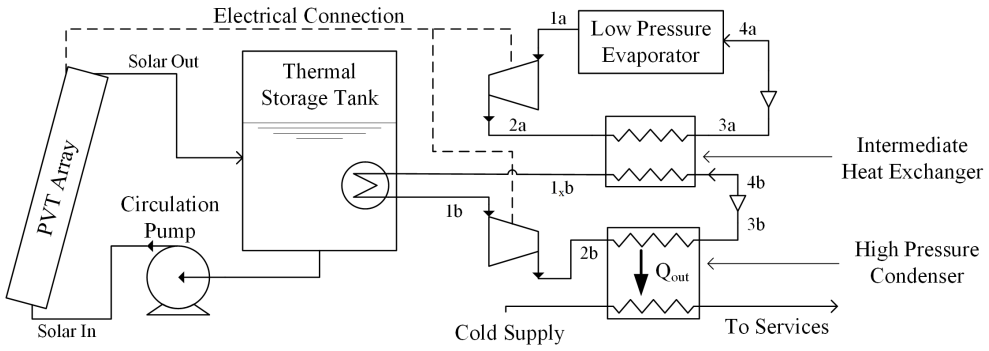

Figure 2: Cascade PVT Heating System Schematic

4.1.1 Setting the System Parameters

To begin the analysis, the geographical location of the simulated site must be selected. The local latitude (L_{local}), and longitude (l_{local}) must be determined. The longitude of the local standard time meridian (l_{ST}) must also be determined. Weather data for the selected simulation site must be acquired, which must include the hourly total horizontal irradiation (I_h), diffuse horizontal irradiation ($I_{d,h}$), direct beam irradiation ($I_{b,n}$), and air dry-bulb temperature (T_a).

Next, the total solar collector area (A), collector cooling fluid flow rate ($\dot{m}_f$), solar collector array tilt angle (β), and the solar collector array azimuth angle (a_w) must be set. The minimum operating temperature for the thermal storage tank ($T_{tank_{min}}$), the design heat transfer rate for the evaporator within the thermal storage tank ($\dot{Q}_{HX2_{design}}$), and the thermal storage tank thermal mass ($mc_{p_{tank}}$) are also set at this point.

Since heat pumps are required in the design, the heat pump refrigerant type must be set, along with the selection of the saturation temperatures for each of the heat exchangers within the heat pump loops. The desired degree of superheat of the refrigerant at the state before the compressor in each heat pump loop (i.e. states *1a* and *1b* in Figure 2), and the degree of sub-

cooling of the refrigerant at the state exiting the condenser (i.e. states *3a* and *3b* in Figure 2), must also be set. Finally, the third-order compressor performance coefficients, along with the state information for the manufacturer test data, must be determined from manufacturer data for each of the compressors used in the system.

4.1.2 Defining the "Map" and "Design" Systems

The third-order compressor performance coefficients used in this analysis follow ANSI/AHRI standard 540 [19], and are used in a polynomial fit to compressor performance data based on manufacturer mapping tests. These tests are typically conducted using a prescribed amount of superheating and sub-cooling in the heat pump process, and the predicted compressor performance that is generated from the provided polynomial fit will effectively assume the same amounts of superheating and sub-cooling. Therefore, the compressor performance and corresponding heat pump state information that is found by directly using the manufacturer provided polynomial fits are referred to as the "map" system parameters because they inherently assume the same amounts of superheating and sub-cooling that the manufacture mapping tests assume.

However, the system parameter assumptions that generated the "map" states may differ from those that are desired. To account for these differences, an adjustment to the "map" compressor performance parameters can be carried out. This adjustment of the "map" performance parameters produces results that correspond to the desired system's design, and are therefore defined as the "design" system parameters.

4.1.3 Determining Heat Pump Cycle Enthalpies

Using the system parameters that were set in Section 4.1.1, the enthalpies of the refrigerant through the heat pump loops can be found. As shown in Figure 3, State 1 is defined as the state of the refrigerant before it enters the compressor, State 2 is defined as the state of the refrigerant as it exits the compressor, State 3 is defined as the state of the refrigerant as it exits the condenser, and State 4 is defined as the state of the refrigerant as it exits the throttling valve. Pressure changes through heat exchangers, along with the enthalpy changes through the piping that connects each component, are neglected in this analysis [20].

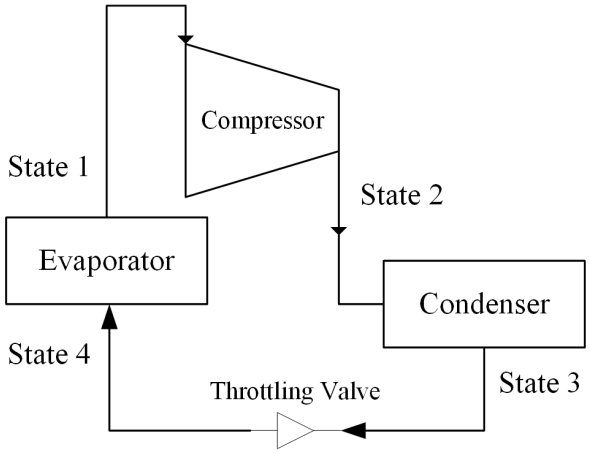

Figure 3: Heat Pump Schematic with Labelled States

Using the saturation temperatures that were set in Section 4.1.1, state information is found for both heat pump loops in the system. This state information must be found for both the mapped system, using "*map*" system state specifications, and design system, using "*design*" system state specifications. In the discussions that follow, since state parameters must be found for both the "*design*" and "*map*" systems, the subscript "*sys*" is used as a placeholder for "*design*" or "*map*" in variable subscripts.

If there is no superheating for State 1, then the enthalpy at State 1 must be found using Equation (1.1). However, if there is superheating, then Equation (1.2) must be used. Next, using the State 1 enthalpy result, Equations (2) and (3) can be used to find the density and specific entropy at State 1, respectively.

$$h_{1_{sys}} = h\left(P_{evap}, x_{sys}\right) \tag{1.1}$$

$$h_{1_{\mathrm{sys}}} = h(P_{evap}, T_{1_{\mathrm{sys}}}) \tag{1.2}$$

$$\rho_{1_{sys}} = \rho(P_{evap}, h_{1_{sys}}) \tag{2}$$

$$s_{1_{sys}} = s(P_{evap}, h_{1_{sys}}) \tag{3}$$

where $h_{1_{sys}}$ is the specific enthalpy at State 1 for the corresponding system (i.e. the "*design"* or "*map"* system), P_{evap} is the saturation pressure at State 1, x_{sys} is the vapour quality at State 1 for the corresponding system, $T_{1_{sys}}$ is the temperature at State 1 for the corresponding system, $\rho_{1_{sys}}$ is the density at State 1 for the corresponding system, and $s_{1_{sys}}$ is the specific entropy at State 1 for the corresponding system.

Next, the isentropic State 2 must be found for both the *design* system, and the *map* system, using Equation (4).

$$h_{2s_{\mathrm{sys}}} = h(P_{cond}, s_{1_{\mathrm{sys}}}) \tag{4}$$

where $h_{2s_{sys}}$ is the specific enthalpy of the isentropic State 2 for the corresponding system, and P_{cond} is the saturation pressure of the refrigerant in the condenser. The isentropic State 2 represents the specific enthalpy of the working fluid after being compressed from the evaporator saturation pressure to the condenser saturation pressure, with constant entropy.

The mapped compressor power consumption and mass flow rate are calculated at this point. This calculation is completed using Equation (5), and using the compressor performance coefficients that were previously acquired from manufacturer data.

$$X_{map} = C_1 + C_2S + C_3D + C_4S^2 + C_5SD + C_6D^2 + C_7S^3 + C_8DS^2 + C_9SD^2 + C_{10}D^3 \quad (5)$$

where X_{map} is the parameter being calculated (i.e. mapped power consumption ($\dot{W}_{map}$) or mapped mass flow rate ($\dot{M}_{map}$)), S is the saturation temperature of the refrigerant on the suction side of the compressor, D is the saturation temperature of the refrigerant on the discharge side of the compressor and $C_1, C_2, \dots, C_{10}$ are the corresponding compressor performance coefficients for the given parameter X_{map}.

Since the performance parameter that was calculated using Equation (5) corresponds to the performance at the mapped state, the previously mentioned adjustment to the performance parameter must be made. To complete this adjustment a new mass flow rate must first be calculated using Equation (6) [21].

$$\dot{M}_{design} = \dot{M}_{map} \times \left(1 + F\left(\frac{\rho_{1_{design}}}{\rho_{1_{map}}} - 1\right)\right) \quad (6)$$

where $\dot{M}_{design}$ is the adjusted mass flow rate for the design system, and F is a chosen percentage of the theoretical mass flow rate increase. The chosen percentage of the theoretical mass flow rate increase can be taken as 0.75 based on findings in the literature [21].

Using the adjusted mass flow rate, and previously determined enthalpy values, a modified compressor power consumption can be found using Equation (7) [21].

$$\dot{W}_{mod} = \dot{W}_{map} \times \left(\frac{\dot{M}_{new}}{\dot{M}_{map}}\right)\left(\frac{h_{2s_{design}} - h_{1_{\text{design}}}}{h_{2s,map} - h_{1,map}}\right) \quad (7)$$

where $\dot{W}_{mod}$ is the modified compressor power consumption for the design system.

The result of Equation (7) typically over-predicts the change in power consumption from the mapped system to the design system by about 48%, based on experimental data found in the literature [21]. According to Dabiri et al. [21], this over-prediction occurs because State 1, which is equal to the state at the evaporator outlet and compressor shell inlet, is used in Equation (7). However, more accurate results can be achieved if the state at the compressor suction port is used instead. The calculation of the state at the compressor suction port requires additional information about the compressor being analyzed, which is not typically available, and therefore the less accurate state value was selected for use in Equation (7). Therefore, a generalized correction to alleviate this over-prediction was used in this analysis, and is shown in Equation (8).

$$\dot{W}_{new} = \dot{W}_{map} + \left(\dot{W}_{mod} - \dot{W}_{map}\right)\times 0.52 \tag{8}$$

where $\dot{W}_{new}$ is the corrected compressor power consumption.

At this point, the actual specific enthalpy of the working fluid after the compressor for the design system can be found using Equation (9).

$$h_{2_{\text{design}}} = \left(\frac{\dot{W}_{new}}{\dot{M}_{new}}\right) + h_{1_{design}} \tag{9}$$

where $h_{2_{\text{design}}}$ is the actual specific enthalpy of the working fluid after the compressor for the design system.

It is prudent to check that the isentropic efficiency of the compressor does not exceed unity since this would indicate an error in the preceding analysis. The isentropic efficiency of the compressor in the corresponding system (η_{sys}) can be found using Equation (10).

$$\eta_{sys} = \frac{h_{2s_{\text{sys}}} - h_{1_{sys}}}{h_{2_{\text{sys}}} - h_{1_{sys}}} = \frac{h_{2s_{\text{sys}}} - h_{1_{sys}}}{\dot{W}_{sys}/\dot{M}_{sys}} \quad (10)$$

Now, the specific enthalpy of the working fluid at State 3 in the *design* system ($h_{3_{\text{design}}}$) must be found using Equation (11) if there is no sub-cooling, or Equation (11.2) if there is sub-cooling.

$$h_{3_{\text{design}}} = h(P_{cond}, x_{3_{design}}) \quad (11.1)$$

$$h_{3_{\text{design}}} = h(P_{cond}, T_{3_{design}}) \quad (11.2)$$

where $x_{3_{design}}$ is the quality of the working fluid at State 3 in the design system, and $T_{3_{design}}$ is the temperature of the working fluid at State 3 in the design system.

The last state in each heat pump loop, State 4, has the same specific enthalpy as State 3 (i.e. $h_{4_{\text{design}}} = h_{3_{\text{design}}}$). This equality is used because it is assumed that the throttling process from State 3 to State 4 is a constant enthalpy process [22].

4.1.4 Time Dependent Parameter Calculations

Once all location and heat pump enthalpy parameters are determined for the system, the time dependent parameters can be calculated. To begin this process, the initial conditions for the system must be set. The system is assumed to not operate during the first simulation time-step, and therefore the mass flow rates in all heat pump loops are set to zero (i.e. $m_{RA_1} = m_{RB_1} = 0$). The temperature of the thermal storage tank, along with the solar panel fluid inlet, and outlet temperatures, are all set to the minimum thermal storage tank temperature (i.e. $T_{tank_1} = T_{in_1} = T_{out_1} = T_{tank_{min}}$, respectively).

Following setting the initial conditions for the system, the iterative segment of the simulation can begin. The goal of the following calculations is to determine the thermal storage

tank temperature (T_{tank}), and heat energy output from the condenser in loop RB (Q_{cond_b}) for each time-step in the simulation. Therefore, the proceeding parameters must all be determined at each time-step until the simulation is complete.

The process begins by first checking if there is solar irradiation at the current time-step. This determination is completed by checking if direct beam solar irradiation is present at the current time-step, based on the input weather data (i.e. check if $I_{b,n_i} > 0$). If there is no direct beam irradiation, then the system does not operate, resulting in the heat output from the condenser in loop RB being zero at the current time-step, and the thermal storage tank being set to the temperature from the previous time-step. The next time-step can then be started by again checking if direct beam solar irradiation is present.

If there is direct beam solar irradiation present at the current time-step, the calculation of all system parameters is carried out. This calculation begins by first determining the solar altitude angle (α) and solar azimuth angle (α_s), which are shown in Figure 4.

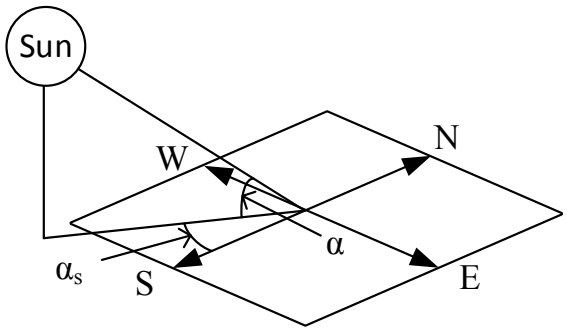

Figure 4: Sun Angle Diagram

To determine the solar altitude and azimuth angles, the solar declination angle (δ_{s_i}) must first be determined using Equation (12) [23].

$$\delta_{s_i} = 23.45° \sin\left(360° \times \frac{284 + n_i}{365}\right) \quad (12)$$

where n_i is the day number at the current time-step. For the day number, January 1st is defined as $n = 1$.

At this point, the value of the equation of time (ET_i) at the current time-step must be determined using Equation (13) and Equation (14) [23].

$$ET_i = 9.87\sin(2B_i) - 7.53\cos(B_i) - 1.5\sin(B_i) \quad (13)$$

$$B_i = 360° \times \left(\frac{n_i - 81}{364}\right) \quad (14)$$

Next, the solar time at the current time-step (ST_i), which is the number of minutes before or after local solar noon, based on the standard time clock, must be determined using Equation (15) [23].

$$ST_i = LST_i + ET_i + (l_{ST} - l_{local}) \times 4 \left(\frac{minutes}{degree}\right) \quad (15)$$

where LST_i is the local standard time at the current time-step, l_{ST} is the longitude at the local corresponding standard time meridian, and l_{local} is the local longitude. Equation (15) assumes that a location in the Western hemisphere is used, and that Western longitude values are positive. Finally, for both the solar time and local standard time, a negative value is used at times before local solar noon, and a positive value is used at times after local solar noon.

The solar altitude angle at the current time-step (α_i) can now be found using Equation (16) [23].

$$\sin(\alpha_i) = \sin(L) \times \sin(\delta_{s_i}) + \cos(L) \times \cos(\delta_{s_i}) \times \cos\left(\frac{ST_i}{4}\right) \quad (16)$$

where L is the local latitude.

The solar azimuth angle at the current time-step (α_{s_i}) can be found at this point by using both Equation (17) and Equation (18) [24].

$$\alpha_{s_i} = \text{acos}\left[\frac{\sin(L)\sin(\alpha_i) - \sin(\delta_{s_i})}{\cos(L)\cos(\alpha_i)}\right] \tag{17}$$

$$\sin(\alpha_{s_i}) = \frac{\cos(\delta_{s_i})\sin\left(\frac{ST_i}{4}\right)}{\cos(\alpha_i)} \tag{18}$$

Two redundant equations are required to determine the solar azimuth angle such that the quadrant that the angle lies in can be determined. If the result of Equation (18) is positive, then the solar azimuth angle is set equal to the result of Equation (17). Alternatively, if the result of Equation (18) is negative, then the solar azimuth angle is set equal to the negative result of Equation (17).

Next, the angle between the solar collector array surface normal vector and the incident solar irradiation at the current time-step, which is defined as the solar incidence angle (i_{c_i}), must be found using Equation (19) [23]:

$$i_{c_i} = \text{acos}\left[\cos(\alpha_i)\cos\left(\alpha_{s_i} - a_w\right)\sin(\beta) + \sin(\alpha_i)\cos(\beta)\right] \tag{19}$$

where a_w is the panel azimuth angle, and β is the panel tilt angle.

The total solar irradiation on the solar collector at the current time-step (I_{c_i}) can be determined at this point. The total solar irradiation on the collector is composed of beam irradiation, diffuse sky irradiation, and reflected irradiation. The total collector irradiation can then be found based on this assumption using Equation (20).

$$I_{c_i} = I_{b,n_i}\cos(i_{c_i}) + I_{d,h_i}\cos^2\left(\frac{\beta}{2}\right) + \rho_i I_{h_i}\sin^2\left(\frac{\beta}{2}\right) \tag{20}$$

where $I_{d,h}$ is the diffuse horizontal irradiation at the current time-step from weather data, ρ_i is the ground reflectivity at the current time-step from weather data, and I_{h_i} is the total horizontal irradiation at the current time-step from weather data.

The total incident solar energy over the current time-step (E_i) can be found at this point using Equation (21).

$$E_i = I_{c_i} \times A \times \Delta t \tag{21}$$

where A is the total solar collector array absorber area, and Δt is the time-step length.

Next, the fluid inlet temperature to the solar collector array at the current time-step (T_{in_i}), is set equal to the thermal storage tank temperature from the previous time-step, as shown in Equation (22).

$$T_{in_i} = T_{tank_{i-1}} \tag{22}$$

where $T_{tank_{i-1}}$ is the temperature of the thermal storage tank from the previous time-step.

Next, the mean temperature of the solar collector array at the current time-step (T_{m_i}) is found using Equation (23).

$$T_{m_i} = \frac{T_{in_i} + T_{out_{i-1}}}{2} \tag{23}$$

where $T_{out_{i-1}}$is the temperature of the fluid exiting the solar collector array at the previous time-step.

The incident angle modifier at the current time-step (φ_i), must now be found using the correlation provided by the panel manufacturer, and is a function of the solar incidence angle. This parameter represents the performance of the solar collector as a function of the solar incidence angle, and is required since many solar collectors exhibit varying performance given a constant solar flux and changing solar incidence angle. Equation (24) is the function that was derived for the Solimpeks PowerTherm PVT panel [25].

$$\varphi_i = -3.04\times10^{-8}\times\left|i_{c_i}\right|^4 + 2.63\times10^{-6}\times\left|i_{c_i}\right|^3 - 1.36\times10^{-4}\times\left|i_{c_i}\right|^2 + 2.02\times10^{-3}\times\left|i_{c_i}\right| + 1 \quad (24)$$

Next, using the mean temperature of the solar array, along with correlations from manufacturer data, the electrical efficiency of the solar collector array at the current time-step (η_{e_i}) can be found. Equation (25) is the function that was derived for Solimpeks PowerTherm PVT panel [25].

$$\eta_{e_i} = \varphi_i\times\frac{\left(186.6 - 0.6771\times T_{m_i}\right)}{1400} \quad (25)$$

After determining the electrical efficiency of the array, the thermal efficiency of the array at the current time-step (η_{th_i}) can be determined. The thermal efficiency is determined using a second order efficiency curve along with the panel reduced temperature (T_{r_i}) at the current time-step. The panel reduced temperature is first determined using Equation (26).

$$T_{r_i} = \frac{T_{m_i} - T_{a_i}}{I_{c_i}} \quad (26)$$

where T_{a_i} is the air dry bulb temperature at the current time-step from weather data.

Using the panel reduced temperature, the thermal efficiency of the array can be found using Equation (27), which is the function that was derived for the Solimpeks PowerTherm PVT panel [25].

$$\eta_{th_i} = \varphi_i\times(0.493 - 4.086\times T_{r_i} - 0.068\times I_{c_i}\times T_{r_i}^2) \quad (27)$$

In time-steps where the resulting array thermal efficiency is a negative value, the thermal efficiency is set to zero and the system is assumed to not operate. This case can occur when there is low thermal irradiation coupled with outdoor temperatures that are low compared to the panel temperature.

Next, the total thermal energy generation (E_{th_i}) and electrical energy generation (E_{e_i}) over the current time-step can be found using Equation (28) and Equation (29), respectively.

$$E_{th_i} = \eta_{th_i} \times E_i \tag{28}$$

$$E_{e_i} = \eta_{e_i} \times E_i \tag{29}$$

Using the resulting thermal energy generated over a time-step, the outlet temperature of the fluid passing through the solar array over the current time-step (T_{out_i}) can be determined with Equation (30).

$$T_{out_i} = T_{in_i} + \frac{E_{th_i}}{\Delta t \dot{m}_f c_p} \tag{30}$$

where $\dot{m}_f$ is the total mass flow rate of fluid through the solar collector array, and c_p is the specific heat capacity of that fluid.

At this point, the heat extracted from the thermal storage tank over the time-step can be considered. Since the system is assumed to operate with a minimum thermal storage tank temperature, at times when the tank is below this temperature, the heat pump loops do not operate. This non-operating state results in the refrigerant total mass flows over the time-step in both heat pump loops RA (m_{RA}) and RB (m_{RB}) being set to zero. The amount of heat extracted through HX2 ($Q_{HX2_{actual_i}}$) and the amount of heat rejected through the condenser in loop RB ($Q_{cond_{b_i}}$) are then also set to zero. The temperature of the thermal storage tank at the current time-step (T_{tank_i}) can then be found using Equation (31).

$$T_{tank_i} = T_{tank_{i-1}} + \frac{E_{th_i}}{\left(mc_p\right)_{tank}} \tag{31}$$

where $\left(mc_p\right)_{tank}$ is the thermal mass of the thermal storage tank.

Alternatively, for the case when the thermal storage tank is of sufficient temperature, and there is solar irradiation present, the calculation of the heat pump operating parameters can be carried out. At the beginning of this analysis a design heat transfer rate for HX2 ($\dot{Q}_{HX2_{design}}$) was selected, and based on this rate the maximum thermal energy that can be extracted from the thermal storage tank over the current time-step ($Q_{HX2_{max_i}}$) can be found using Equation (32):

$$Q_{HX2_{max_i}} = \dot{Q}_{HX2_{design}} \times \Delta t_{step} \times \left(\frac{T_{tank_{i-1}} - T_{evap_{HX2}}}{T_{tank_{min}} - T_{evap_{HX2}}} \right) \quad (32)$$

Equation (32) assumes that the heat transfer area and the convection coefficient for heat transfer between the thermal storage tank and the loop RB evaporator contained within the thermal storage tank are constant throughout the analysis. This assumption allows for the heat transfer over a time-step to be proportional to the designed heat transfer rate, step length, and the ratio of the current temperature difference between the thermal storage tank and HX2 to the minimum temperature difference the thermal storage tank and HX2. However, during time-steps with low electrical energy production, referred to as the limited electricity state, there is not enough electrical energy to run the compressors in loop RB if the actual heat extraction rate from the thermal storage tank is set equal to $Q_{HX2_{max_i}}$. Therefore, in time-steps during which the system operates in the limited electricity state, HX2 will have more than sufficient heat transfer potential to provide enough heat to balance the cycle. This case allows loop RA to be inactive, and the amount of heat energy that can be transferred through HX2 can be found using Equation (33), which assumes that the compressor power consumption constrains the system.

$$Q_{HX2_{elec_i}} = E_{e_i} \frac{(h_{b1} - h_{b4})}{(h_{b2} - h_{b1})} \quad (33)$$

where $Q_{HX2_{elec_i}}$ is the quantity of thermal energy transferred through HX2 over the current time-step when the system is operating with limited electricity.

The determination whether the system operates with limited electricity, or is fully operational, is achieved by comparing $Q_{HX2_{max_i}}$ and $Q_{HX2_{elec_i}}$. When $Q_{HX2_{elec_i}} > Q_{HX2_{max_i}}$ the system is fully operational, and the actual heat transfer through HX2 ($Q_{HX2_{actual_i}}$) is set to equal to $Q_{HX2_{max_i}}$. Alternatively, when $Q_{HX2_{elec_i}} \leq Q_{HX2_{max_i}}$ the system operates in the limited electricity state, and the actual heat transfer through HX2 is set to be equal to $Q_{HX2_{elec_i}}$.

After the actual heat transfer through HX2 over the current time-step is determined, the mass flow rates of refrigerant, and heat transfer rates through the heat pump loops, can be calculated. When the system operates in the limited electricity case, only loop RB operates, which allows for a direct solution of the total mass flow of refrigerant in loop RB over the current time-step (m_{RB_i}) using Equation (34).

$$m_{RB_i} = \frac{Q_{HX2_{actual_i}}}{h_{b1} - h_{b4}} \tag{34}$$

Next, the heat rejected at the condenser in loop RB over the current time-step ($Q_{cond_{b_i}}$) can be found using Equation (35).

$$Q_{cond_{b_i}} = m_{RB_i}(h_{b2} - h_{b3}) \tag{35}$$

Alternatively, when the system is fully operational, Equation (36) and Equation (37) must be solved simultaneously for the total refrigerant mass flows over the current time-step, for both heat pump loops.

$$(h_{a2} - h_{a1})m_{RA_i} + (h_{b2} - h_{b1})m_{RB_i} = E_{e_i} \tag{36}$$

$$-(h_{a2} - h_{a3})m_{RA_i} + (h_{b1} - h_{b4})m_{RB_i} = E_{th_i} \tag{37}$$

Next, similar to the limited electricity case, the heat rejected at the condenser in loop RB can be found using Equation (35), using the result of the solutions from Equation (36) and Equation (37).

Finally, the time-step concludes by determining the temperature of the thermal storage tank using Equation (38), which accounts for both the heat added by the solar collector fluid, and the heat removed through HX2.

$$T_{tank_i} = T_{tank_{i-1}} + \frac{E_{th_i} - Q_{HX2_{actual_i}}}{\left(mc_p\right)_{tank}} \tag{38}$$

In Section 5, a case study that implemented the previously detailed analysis technique will be presented, such that the efficacy of the PVT cascade heat pump system can be discussed.

5 Case Study Parameters and Results

A case study was carried out that compared the total annual energy output from the PVT cascade heat pump system to the simultaneous consumption PVT heat pump system, and the next leading solar domestic hot water system in the market, which was found to be the evacuated tube water heating system [3]. The design parameters that were used in comparing all systems were suitable for 60°C domestic hot water production. Several locations were used, such that the effects of different climate could be determined. Table 1 presents a summary of the locations that were considered, along with related basic climate data [26, 27].

Table 1: Case Study Locations with Climate Data

Location (City, Country)	Location Latitude	Annual Average Dry-Bulb Temperature (°C)	Total Annual Solar Beam Irradiation (kWh/m^2)
Edmonton, Canada	53.6°	2.8	1491
Toronto, Canada	43.7°	7.4	1252
Washington DC, USA	39.0°	12.7	1378
Phoenix, USA	33.5°	23.8	2524

The details and results of the evacuated tube analysis will be presented first, since they will be used as the base case for the comparison to the other two systems. The simulation results

from the simultaneous consumption PVT heat pump system, and the PVT cascade heat pump system, will then be given.

5.1 Evacuated Tube Water Heating System

A schematic of the evacuated tube water heating system that was used in this study is shown in Figure 5.

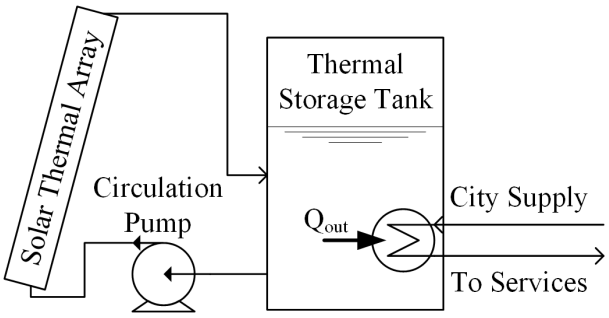

Figure 5: Evacuated Tube Heating System Schematic

The thermal storage tank in this system was assumed to have a constant temperature of 65°C, which ensures that hot water at a temperature of 60°C can be produced from the city supply water that passes through the heat exchanger in the thermal storage tank. The mass flow rate of the city supply water was assumed to be variable, such that the heat removed from the thermal storage tank by the city supply water would allow the temperature of the thermal storage tank to be kept constant. Finally, since the desired output of this analysis was the energy output profile to the city supply water, the resulting required mass flow rate and inlet temperature of the city supply water were not needed.

The analysis of the evacuated tube system was also carried out using the process that was described in Section 4, but neglecting the heat pump calculations since heat pumps were not included in this system. A Solar Panels Plus SPP-30 evacuated tube solar collector was used in

this analysis, and the incidence angle modifier and thermal efficiency equations that were used to model this collector are shown in Equation (39) and Equation (40), respectively [28]. The remaining simulation input parameters for the evacuated tube analysis are shown in Table 2.

$$\varphi_i = -4\times10^{-7}\times\left|i_{c_i}\right|^4 + 3\times10^{-5}\times\left|i_{c_i}\right|^3 - 6\times10^{-4}\times\left|i_{c_i}\right|^2 + 6.3\times10^{-3}\times\left|i_{c_i}\right| + 1 \quad (39)$$

$$\eta_{th_i} = \varphi_i\times(0.477 - 0.9374\times T_{r_i} - 0.00655\times I_{c_i}\times T_{r_i}^2) \quad (40)$$

Table 2: Design Input Parameters for Evacuated Tube System Case Study

Parameter	**Value**
Time-step length.	$60\ s$
Total array absorber area	$8.4\ m^2$
Thermal storage tank thermal mass	$16.72\frac{MJ}{K}$
Fluid mass flow rate through solar collector array	$0.17\frac{kg}{s}$
Panel azimuth angle	0°
Specific heat capacity of solar array cooling fluid.	$4180\frac{J}{kgK}$

The optimization process was carried out by running a simulation in each location using panel tilt angles ranging from 0° to 90°, then, for each location, selecting the panel tilt angle that resulted in the maximum thermal energy output over the simulated year. A plot of the results from the tilt angle optimization is shown in Figure 6.

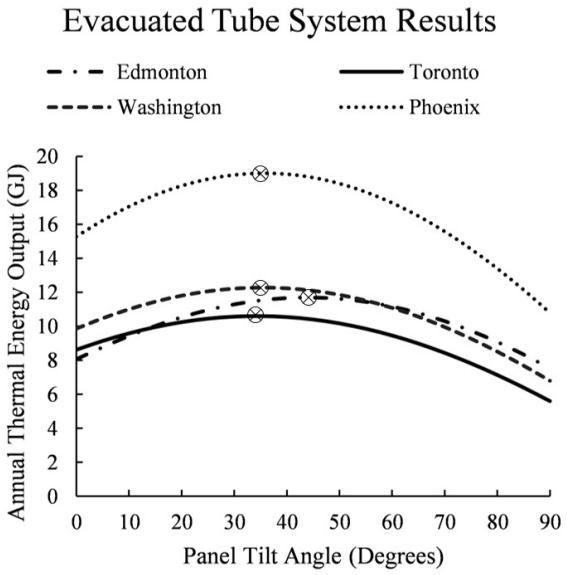

480

481 Figure 6: Evacuated Tube Annual Thermal Output vs. Panel Tilt Angle
482

483 For illustration purposes, a sample plot showing a resulting thermal power output profile
484 for a simulated year in Toronto is shown in Figure 7, which was generated using a panel tilt
485 angle of 35°.

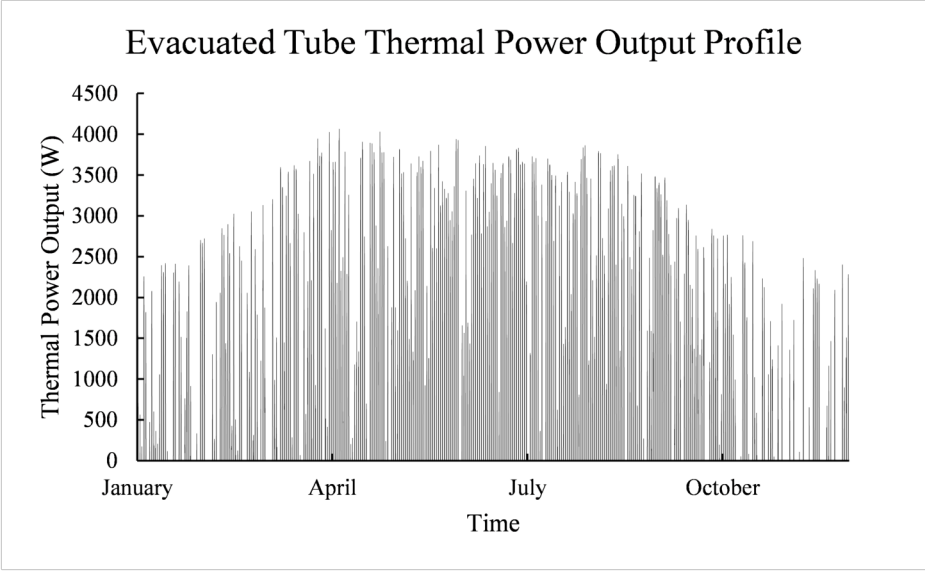

486
487 Figure 7: Evacuated Tube Sample Thermal Power Output Profile
488

After running the simulation at each location, and varying the panel tilt angle, the panel tilt angle that resulted in the maximum annual thermal energy output was determined. This optimal tilt angle is represented by the local maxima of each curve in Figure 6, and is marked on each curve in the plot for clarity. The resulting optimal tilt angle for each location, and the corresponding annual energy outputs, are presented in Table 3.

Table 3: Evacuated Tube System Analysis Results

Location (City, Country)	Optimal Tilt Angle	Corresponding Annual Thermal Energy Output (GJ)
Edmonton, Canada	44°	11.7
Toronto, Canada	34°	10.6
Washington DC, USA	35°	12.3
Phoenix, USA	36°	19.0

The optimal tilt angles that were determined through this optimization process, along with the trends in total annual energy production, were verified using RETScreen software [29]. These results will be used for comparison against both of the PVT heat pump system annual energy outputs in Section 5.4.

5.2 Simultaneous Production PVT Heat Pump System

Several simulations of the simultaneous consumption PVT heat pump system were carried out to determine the operating parameters that result in the highest annual thermal energy output for each simulation location. A schematic that will be used to discuss the process is shown in Figure 8.

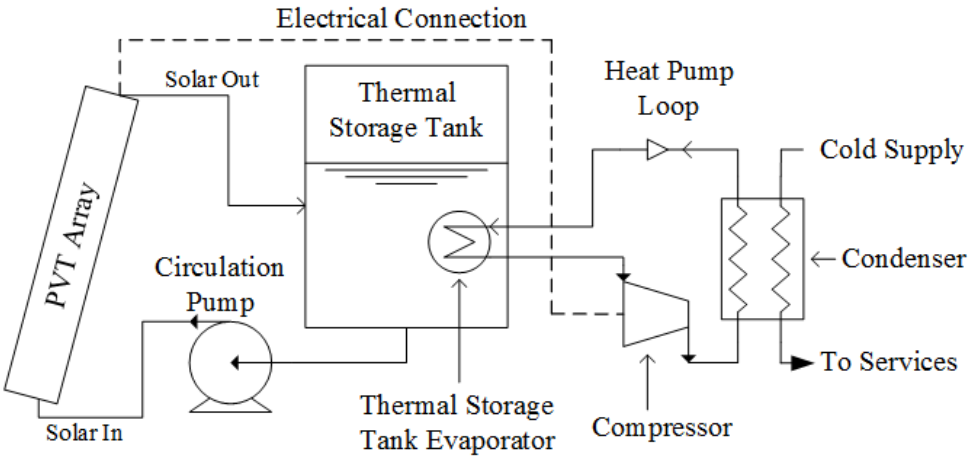

Figure 8: Simultaneous Consumption PVT Heat Pump System Schematic

The panel tilt angle and the minimum thermal storage tank temperature were varied at each location to determine the combination of these two parameters that results in the system's maximum annual thermal energy output. An Emerson Climate ZB15KQE-PFJ variable capacity scroll compressor was used as the compressor in the heat pump loop [30]. REFPROP refrigerant property calculating software [31] was used to determine refrigerant state information for each of the trials, and Table 6 presents the parameters that were kept constant between each of these trials.

Table 4: Design Input Parameters for PVT System Case Study

Parameter	Value
Time-step length.	$60\ s$
Total array absorber area	$8.4\ m^2$
Thermal storage tank thermal mass	$16.72\ MJ/K$
Fluid mass flow rate through solar collector array	$0.18\frac{kg}{s}$
Panel azimuth angle	0°
Heat Pump Evaporator Saturation Temperature	$30°C$
Heat Pump Condenser Saturation Temperature	$65°C$
Design heat transfer rate of the heat exchanger in the thermal storage tank	$1000\ W$ [18]
Heat pump refrigerant type	R-134a
Specific heat capacity of solar panel cooling fluid.	$4180\frac{J}{kgK}$

The optimization process was carried out by first setting the minimum thermal storage tank temperature to 35°C, and varying the panel tilt angle, for each simulation location. Second, using the optimal panel tilt angle that was found during the first step in the optimization process, the minimum thermal storage tank temperature was varied to determine its optimal value for each location. Finally, to ensure that the optimal panel tilt angle did not change, the simulation for each location was re-run, varying the panel tilt angle while using the optimal minimum thermal storage tank temperature that was determined during the second step of the optimization process, to ensure that the optimal tilt angle did not change. A flowchart that represents this process is shown in Figure 9.

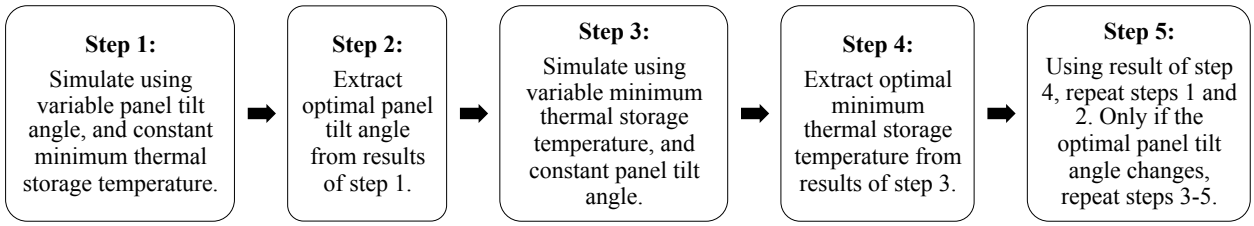

Figure 9: PVT Heat Pump System Optimization Process Flowchart

For illustration purposes, a sample plot showing the resulting thermal storage tank temperature for the simultaneous consumption PVT heat pump system over the simulated year in Toronto is shown in Figure 10, and the corresponding resulting thermal power output profile is shown in Figure 11. The plots in Figure 10 and Figure 11 were generated using a panel tilt angle of 31°, and a minimum thermal storage tank temperature of 24°C.

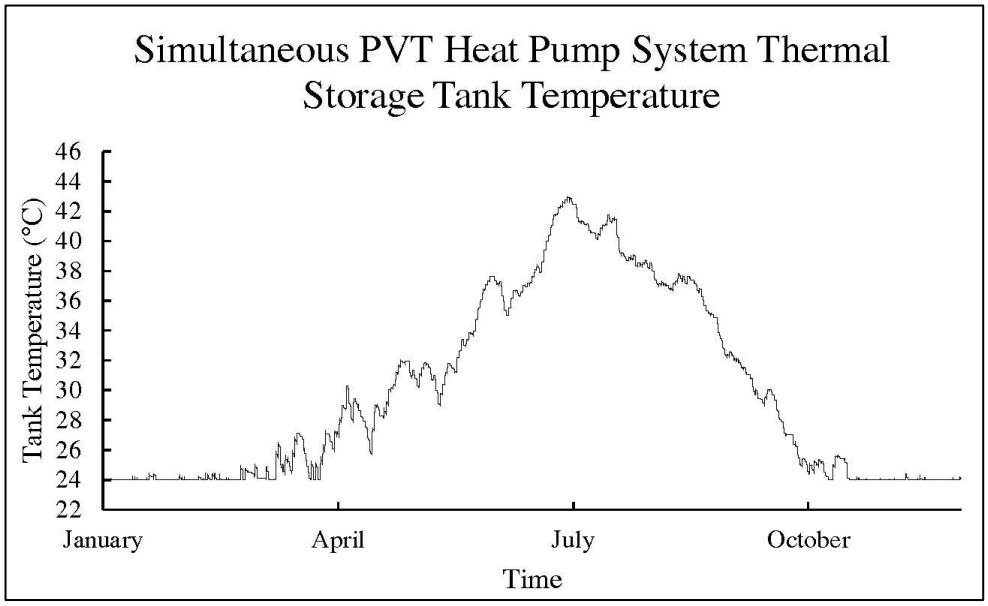

Figure 10: Simultaneous Consumption PVT Heat Pump Sample Thermal Storage Tank Temperature Profile

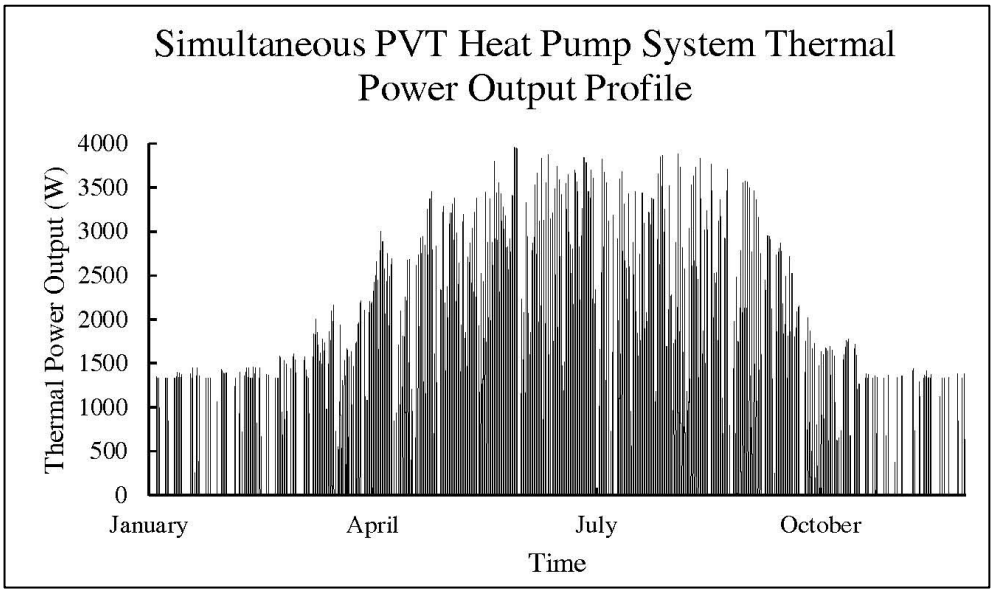

Figure 11: Simultaneous Consumption PVT Heat Pump Sample Thermal Power Output Profile

Based on the results shown in Figure 10, one can conclude that the system operates more frequently from April-October since the thermal storage tank is above the minimum temperature more frequently than in other months. This result is also verified by the higher density thermal power production profile shown in Figure 11 during the months of April-October.

A plot of the results from the panel tilt optimization process is shown in Figure 12a, and a plot of the results from the minimum thermal storage tank optimization process is shown in Figure 12b.

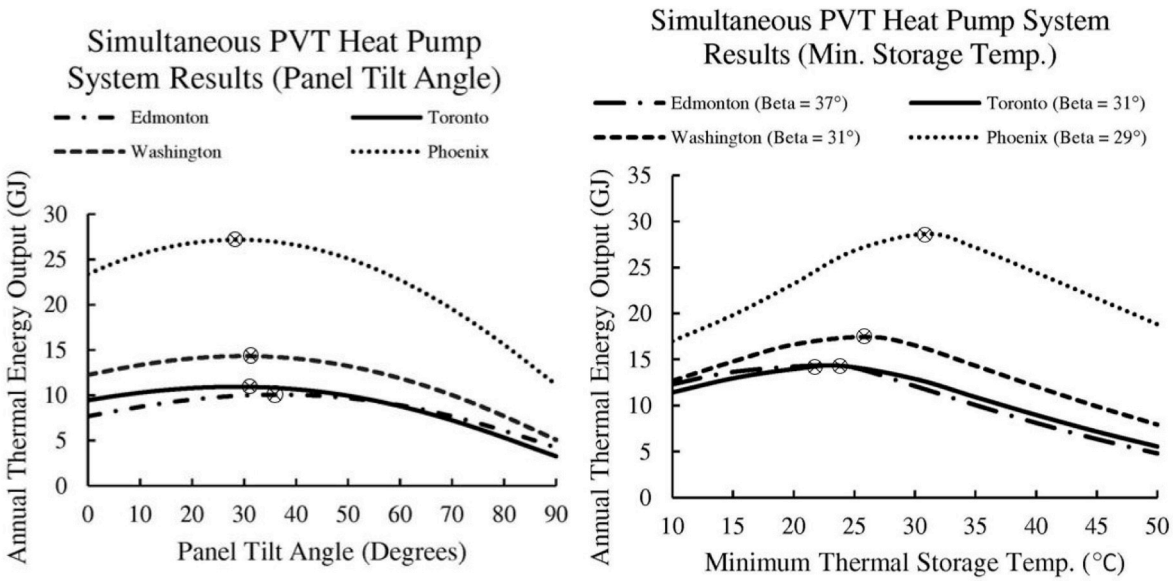

(a) (b)

Figure 12: Simultaneous Consumption PVT Heat Pump Annual Energy Output Plots

Each curve in Figure 12a was generated using a variable panel tilt angle, and a constant thermal storage tank temperature of 35°C. Therefore, the local maxima of each curve in Figure 12a, which is marked on each curve, corresponds to the annual thermal energy output when the optimal panel tilt angle for each simulation location is used, and the thermal storage tank temperature is set to 35°C.

Each curve in Figure 12b was generated using a variable thermal storage tank temperature, and the optimal panel tilt angle for each location, which was found using Figure 12a. Therefore, the local maxima of each curve in Figure 12b, which is marked on each curve, corresponds to the annual thermal energy output when both the optimal thermal storage tank

559 temperature is used, along with the optimal panel tilt angle, and is defined as the optimized
560 value.

561 A summary of the optimal panel tilt angle, optimal minimum thermal storage tank
562 temperature, and the optimized annual thermal energy output of the simultaneous PVT heat
563 pump system for each location is presented in Table 5.

564 Table 5: Simultaneous Consumption PVT Heat Pump System Optimization Results

Location (City, Country)	Optimal Tilt Angle	Optimal Minimum Thermal Storage Tank Temperature	Corresponding Annual Thermal Energy Output (GJ)
Edmonton, Canada	37°	22°C	14.4
Toronto, Canada	31°	24°C	14.3
Washington DC, USA	31°	26°C	17.5
Phoenix, USA	29°	31°C	28.6

565

566 These optimized results will be used for comparison against the evacuated tube system and
567 the PVT cascade heat pump system annual energy outputs in Section 5.4.

568

569 ## 5.3 PVT Cascade Heat Pump System

570 Several simulations of the PVT cascade heat pump system were carried out to determine
571 the operating parameters that result in the highest annual thermal energy output for each
572 simulation location. The panel tilt angle and the minimum thermal storage tank temperature were
573 varied at each location to determine the combination of these two parameters that results in the
574 system's maximum annual thermal energy output. An Emerson Climate ZB15KQE-PFJ variable
575 capacity scroll compressor was used as the compressor in the heat pump loop [32]. REFPROP
576 refrigerant property calculating software [33] was used to determine refrigerant state information
577 for each of the trials, and Table 6 presents the parameters that were kept constant between each
578 of these trials.

579 Table 6: Design Input Parameters for PVT Cascade Heat Pump System Case Study

Parameter	Value
Time-step length.	$60\ s$
Total array absorber area	$8.4\ m^2$
Thermal storage tank thermal mass	$16.72\ MJ/K$
Fluid mass flow rate through solar collector array	$0.18\frac{kg}{s}$
Panel azimuth angle	0°
Heat Pump A Evaporator Saturation Temperature	$5\ °C$
Heat Pump A Condenser Saturation Temperature	$35°C$ [18]
Heat Pump B Evaporator Saturation Temperature	$30°C$
Heat Pump B Condenser Saturation Temperature	$65°C$
Design heat transfer rate of the heat exchanger in the thermal storage tank	$1000\ W$ [18]
Heat pump refrigerant type	R-134a
Specific heat capacity of solar panel cooling fluid.	$4180\frac{J}{kgK}$

580

581 The optimization process was carried out using the same method that was described in
582 Section 5.2 for the simultaneous consumption PVT heat pump system. First, the minimum
583 thermal storage tank temperature was set to 35°C, and the panel tilt angle was varied for each
584 simulation location. Second, using the optimal panel tilt angle that was found during the first step
585 in the optimization process, the minimum thermal storage tank temperature was varied to
586 determine its optimal value for each location. Finally, to ensure that the optimal panel tilt angle
587 did not change, the simulation for each location was re-run, varying the panel tilt angle while
588 using the optimal minimum thermal storage tank temperature that was determined during the
589 second step of the optimization process, to ensure that the optimal tilt angle did not change.

590 For illustration purposes, a sample plot showing the resulting thermal storage tank
591 temperature for the PVT cascade heat pump system over the simulated year in Toronto is shown
592 in Figure 13, and the corresponding resulting thermal power output profile is shown in Figure 14.

The plots in Figure 13 and Figure 14 were generated using a panel tilt angle of 34°, and a minimum thermal storage tank temperature of 28°C.

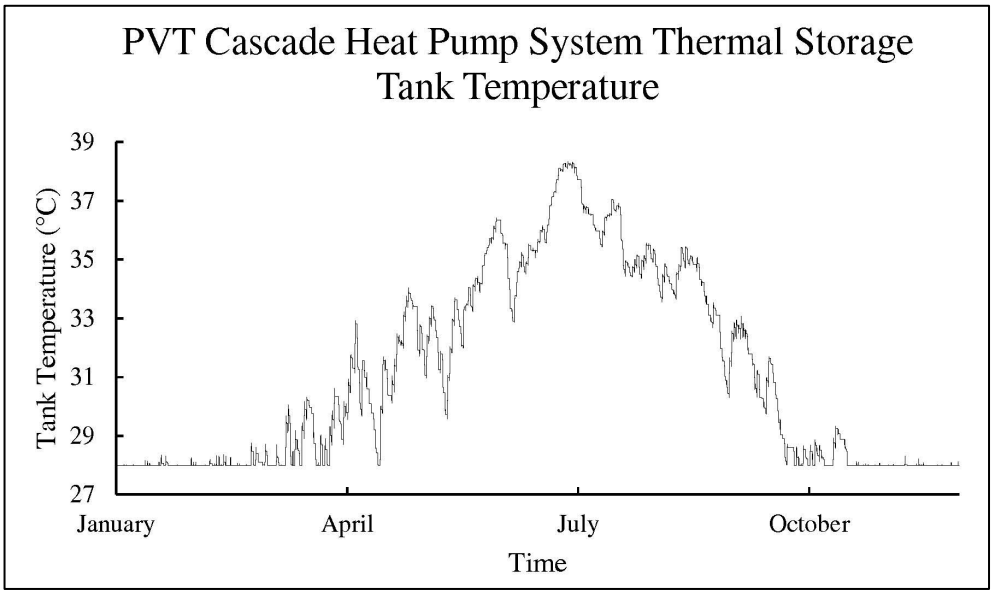

Figure 13: PVT Cascade Heat Pump Sample Thermal Storage Tank Temperature Profile

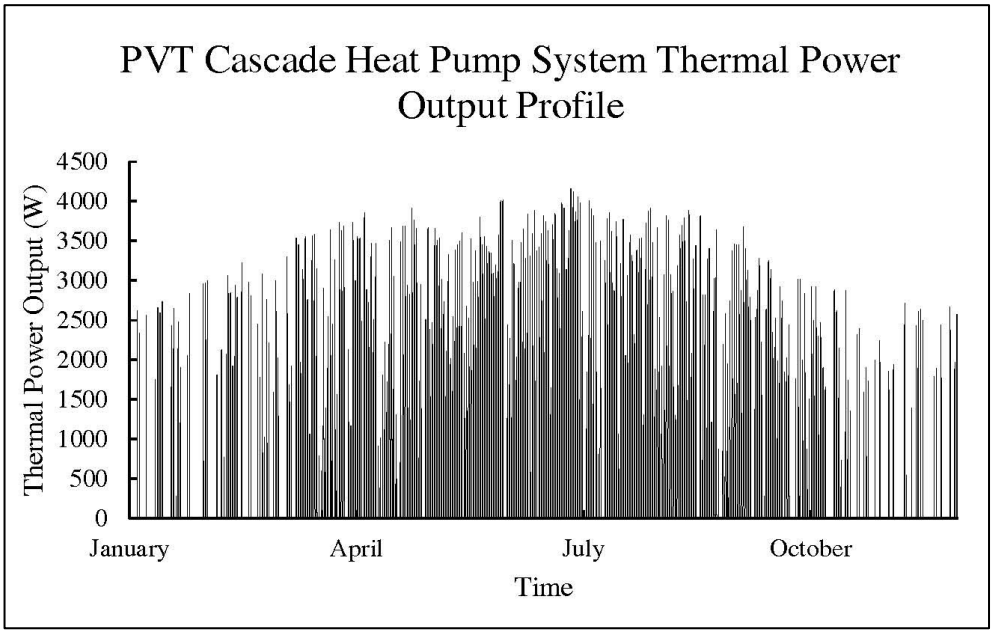

Figure 14: PVT Cascade Heat Pump Sample Thermal Power Output Profile

Using results shown in Figure 13 and Figure 14, and comparable results for the other locations, the total annual thermal energy production based on different panel tilt angles, and

603 minimum thermal storage tank temperatures, was determined for each location. A plot of the
604 results from the panel tilt optimization process is shown in Figure 15a, and a plot of the results
605 from the minimum thermal storage tank optimization process is shown in Figure 15b.

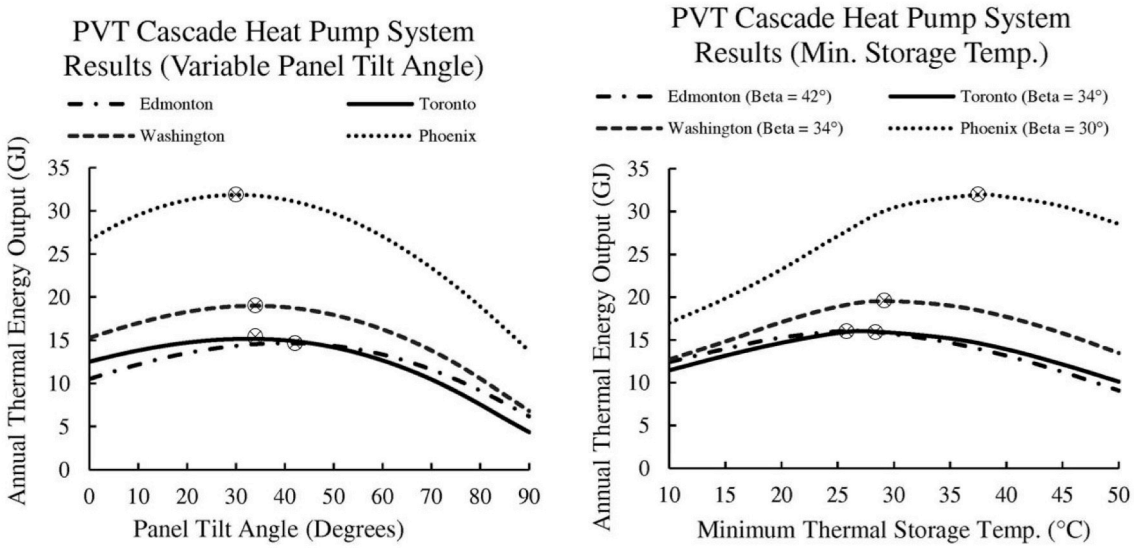

(a) (b)

606 Figure 15: PVT Cascade Heat Pump System Annual Energy Output Plots

607 Since the PVT cascade heat pump system has two operational modes, which are with
608 either one or two heat pumps being active, it is of interest to determine the number of hours spent
609 in each state annually. Table 8 presents these results for the optimized system in each simulation
610 location.

611 Table 7: PVT Cascade Heat Pump Operating Mode Characteristics

Location (City, Country)	Total Annual Operating Hours	Dual Heat Pump Loop Operating Hours	Dual Heat Pump Loop Operating Fraction
Edmonton, Canada	2479	951	38%
Toronto, Canada	2158	936	43%
Washington DC, USA	2925	1059	36%
Phoenix, USA	3463	2009	58%

A summary of the optimal panel tilt angle, optimal minimum thermal storage tank temperature, and the optimized annual thermal energy output of the PVT heat pump system for each location is presented in Table 8.

Table 8: PVT Heat Pump System Optimization Results

Location (City, Country)	Optimal Tilt Angle	Optimal Minimum Thermal Storage Tank Temperature	Annual Thermal Energy Output (GJ)
Edmonton, Canada	42°	26°C	16.1
Toronto, Canada	34°	28°C	16.0
Washington DC, USA	34°	29°C	19.5
Phoenix, USA	30°	37°C	27.1

These optimized results will be used for comparison against the evacuated tube system and the simultaneous PVT heat pump system annual energy outputs in Section 5.4.

5.4 Discussion and Comparison of System Performances

A comparison between the annual energy outputs of the evacuated tube, simultaneous consumption PVT heat pump, and PVT cascade heat pump systems was carried out using the optimized system parameters, as detailed in Sections 5.1, 5.2, and 5.3. Table 9 presents a comparison of these results on both an annual and seasonal basis.

Table 9: Seasonal Comparison between the PVT Heat Pump and Evacuated Tube systems

Location	Date Range	Thermal Energy Output (GJ)			% Difference $100\% \times \left(\frac{E - E_{evac}}{E_{evac}}\right)$	
		Evacuated Tube (E_{evac})	Simultaneous PVT Heat Pump	PVT Cascade Heat Pump	Simultaneous PVT Heat Pump	PVT Cascade Heat Pump
Edmonton, Canada	Jan. 1st – Mar. 31st	2.62	2.04	2.60	-22%	0%
	April 1st – June 30th	3.72	5.61	6.05	50%	62%
	July 1st - Sept. 30th	3.69	5.29	5.71	43%	54%
	Oct. 1st – Dec. 31st	1.65	1.55	1.71	-5%	4%
	Annual	**11.7**	**14.5**	**16.1**	**24%**	**37%**
Toronto, Canada	Jan. 1st – Mar. 31st	2.06	1.60	2.09	-22%	2%
	April 1st – June 30th	3.23	5.27	5.82	62%	79%
	July 1st - Sept. 30th	3.68	5.71	6.19	54%	67%
	Oct. 1st – Dec. 31st	1.62	1.72	1.91	7%	19%
	Annual	**10.6**	**14.3**	**16.0**	**35%**	**51%**
Washington DC, USA	Jan. 1st – Mar. 31st	3.02	2.91	3.74	-4%	24%
	April 1st – June 30th	2.88	5.51	5.89	92%	105%
	July 1st - Sept. 30th	3.35	5.77	6.12	72%	83%
	Oct. 1st – Dec. 31st	3.04	3.28	3.80	8%	25%
	Annual	**12.3**	**17.5**	**19.5**	**42%**	**59%**
Phoenix, USA	Jan. 1st – Mar. 31st	5.22	5.52	6.70	5%	28%
	April 1st – June 30th	3.55	8.21	8.82	133%	150%
	July 1st - Sept. 30th	4.35	8.71	9.27	101%	114%
	Oct. 1st – Dec. 31st	5.89	6.20	7.13	5%	21%
	Annual	**19.0**	**28.6**	**31.9**	**51%**	**68%**

Based on the results presented in Table 9, one can see that in all simulation locations both the simultaneous consumption PVT heat pump, and PVT cascade heat pump system produced more thermal energy than the evacuated tube system, on both a seasonal and annual basis. The PVT cascade heat pump system shows the greatest improvement over both the evacuated tube system, and the simultaneous consumption PVT heat pump system, in locations and during times with higher dry-bulb temperatures.

For example, in Edmonton, which is the simulation location with the lowest annual average dry-bulb temperature, the annual energy output was increased compared to the evacuated tube system by 37%. However, in Toronto, which is the simulation location with the

second lowest annual average dry-bulb temperature, the annual energy output was increased compared to the evacuated tube system by 51%. This further increase in performance continues as the annual average dry-bulb temperature increases for the other simulation locations. Similar trends with the improving annual thermal energy output are seen when comparing the simultaneous consumption PVT heat pump system with the PVT cascade heat pump system. Therefore, based on this trend, the PVT cascade heat pump system offers the most improvement compared to the other two systems in locations with higher dry-bulb temperatures.

A similar result is found when comparing seasons in the same location. For example, in Edmonton, during the Winter months (i.e. January – March) the PVT cascade heat pump system has the same thermal energy output as the evacuated tube system. However, during the Spring months (i.e. April – June), the PVT cascade heat pump system offers an increase in thermal energy output of 62%. This result further supports that the PVT cascade heat pump system offers the greatest improvement during months with higher dry-bulb temperatures. This result also demonstrates that even in a cold climate location, where the dry-bulb temperature and solar insolation are at their lowest annual values (i.e. during the Winter), the PVT cascade heat pump system still generates more thermal energy than the evacuated tube system and simultaneous consumption PVT heat pump system.

A cost estimation was also completed to compare the simultaneous consumption PVT heat pump system to the PVT cascade heat pump system. Since the difference between the equipment required for these two systems is the additional heat pump loop, an incremental cost analysis was completed. The incremental equipment cost associated with adding the secondary heat pump loop is approximately $988 CAD [34, 35, 36, 37]. Assuming that natural gas

664 instantaneous water heaters are used in each location, with an energy factor of 0.90 [38], the
665 annual cost savings shown in Table 10 were calculated.

666 Table 10: Annual Savings Cost Breakdown

Location (City, Country)	Annual Energy Requirement (GJ)	Utility Energy Cost (CAD/GJ)	Yearly Savings (CAD)	Simple Payback Period (years)
Edmonton, Canada	1.89	3.55 [39]	$6.71	147
Toronto, Canada	1.89	3.51[40]	$6.63	149
Washington DC, USA	2.30	15.41 [37, 41]	$35.48	28
Phoenix, USA	3.63	20.97 [37, 41]	$76.15	13

667

668 Based on the estimated payback periods presented in Table 10, and assuming a system
669 lifetime of 20 years [42], the incremental cost of the added heat pump loop is only justified in
670 Phoenix. The long payback periods in Edmonton, Toronto, and Washington are mostly due to the
671 lower cost of natural gas in those locations compared Phoenix. However, the payback periods in
672 all locations may be reduced if the system is mass-produced, and equipment costs can be
673 reduced.

674

675 6 Conclusion

676 A novel PVT cascade heat pump domestic water heating system was presented, along
677 with computer simulation case studies. The system builds on the concepts of other research
678 groups by using two heat pump loops, instead of a single heat pump loop, such that system
679 optimization can be carried out to maximize thermal energy output, and consuming all of the
680 electrical energy generated by the PVT panel. The study was carried out to determine and
681 compare the annual and seasonal energy outputs of the PVT cascade heat pump system with the
682 next leading conventional solar water heating technology, the evacuated tube system, along with
683 a simultaneous consumption PVT heat pump system. The analysis of these systems was carried

684 out using a time-stepping method and manufacturer data. Engineering weather data sets, and heat
685 exchanger temperatures were used as inputs to the model, which yielded thermal power
686 production and temperature profile outputs. Simulations were run using weather data for four
687 different locations, which were Phoenix, Washington, Toronto, and Edmonton. These locations
688 were selected because they provide a range in annual average dry-bulb temperature and total
689 annual solar insolation.

690 Based on the simulations that were completed, it was found that the annual thermal
691 energy output from the PVT cascade heat pump system exceeds the annual thermal energy
692 output of the other two systems at each simulation location. It was also found that at each
693 location, the PVT cascade heat pump system produces equal or more thermal energy than the
694 other two systems during each season of the year. Finally, the PVT cascade heat pump system
695 shows the greatest improvement over the other two systems in locations, and during seasons,
696 with higher dry-bulb temperatures and greater solar insolation. Future research should focus on
697 the development of a prototype, small-scale PVT heat pump apparatus for experimental testing
698 and verification.

---

[1] Kamyar Tanha, Alan S. Fung, Rakesh Kumar, Performance of two domestic solar water heaters with drain water heat recovery units: Simulation and experimental investigation, Applied Thermal Engineering, Volume 90, 5 November 2015, Pages 444-459

[2] Mahmut Sami Buker, Saffa B. Riffat, Solar assisted heat pump systems for low temperature water heating applications: A systematic review, Renewable and Sustainable Energy Reviews, Volume 55, March 2016, Pages 399-413

[3] Zhangyuan Wang, Wansheng Yang, Feng Qiu, Xiangmei Zhang, Xudong Zhao, Solar water heating: From theory, application, marketing and research, Renewable and Sustainable Energy Reviews, Volume 41, January 2015, Pages 68-84

[4] S. S. Bertsch and E. A. Groll, "Two-stage air-source heat pump for residential heating and cooling applications in northern U.S. climates," *International Journal of Refrigeration,* no. 31, pp. 1282-1292, 2008.

[5] H. W. Jung, H. Kang, W. J. Yoon and Y. Kim, "Performance comparison between a single-stage and a cascade multi-functional heat pump for both air heating and hot water supply," International Journal of Refrigeration, no. 36, pp. 1431-1441, 2013.

[6] M. Izquierdo and P. d. Agustín-Camacho, "Solar heating by radiant floor: Experimental results and emission reduction obtained with a micro photovoltaic–heat pump system," Applied Energy, vol. 147, pp. 297-307, 2015.

[7] Raghad S. Kamel, Alan S. Fung, Peter R.H. Dash, Solar systems and their integration with heat pumps: A review, Energy and Buildings, Volume 87, 1 January 2015, Pages 395-412, ISSN 0378-7788, http://dx.doi.org/10.1016/j.enbuild.2014.11.030.

[8] H. Chena, S. B. Riffata and Y. Fu, "Experimental study on a hybrid photovoltaic/heat pump system," Applied Thermal Engineering, vol. 31, pp. 4132-4138, 2011.

[9] Fathabadi, H. (2015). Increasing energy efficiency of PV-converter-battery section of standalone building integrated photovoltaic systems. Energy and Buildings, 101, 1-11.

[10] Carsen J. Banister, Michael R. Collins, Development and performance of a dual tank solar-assisted heat pump system, Applied Energy, Volume 149, 1 July 2015, Pages 125-132, ISSN 0306-2619, http://dx.doi.org/10.1016/j.apenergy.2015.03.130.

[11] Z. M. Amin and M. Hawlader, "Analysis of solar desalination system using heat pump," Renewable Energy, vol. 74, pp. 116-123, 2015.

[12] G. Xu, S. Deng, X. Zhang, L. Yang and Y. Zhang, "Simulation of a photovoltaic/thermal heat pump system having a modified collector/evaporator," Solar Energy, vol. 83, pp. 1967-1976, 2009.

[13] J. Jie, L. Keliang, C. Tin-tai, P. Gang, H. Wei and H. Hanfeng, "Performance analysis of a photovoltaic heat pump," Applied Energy, vol. 85, pp. 680-693, 2008.

[14] G. Xu, X. Zhang and S. Deng, "Experimental study on the operating characteristics of a novel low-concentrating solar photovoltaic/thermal integrated heat pump water heating system," Applied Thermal Engineering, no. 31, pp. 3689-3695, 2011.

[15] X. Zhang, X. Zhao, J. Shen, J. Xu and X. Yu, "Dynamic performance of a novel solar photovoltaic/loop-heat-pipe heat pump system," Applied Energy, vol. 114, pp. 335-352, 2014.

[16] X. Zhang, X. Zhao, J. Xu and X. Yu, "Characterization of a solar photovoltaic/loop-heat-pipe heat pump water heating system," Applied Energy, vol. 102, pp. 1229-1245, 2013.

[17] X. Zhang, J. Shen, P. Xu, X. Zhao and Y. Xu, "Socio-economic performance of a novel solar photovoltaic/loop-heat-pipe heat pump water heating system in three different climatic regions," Applied Energy, vol. 135, pp. 20-34, 2014.

[18] J.P. Fine, J. Friedman, S.B. Dworkin, Transient analysis of a photovoltaic thermal heat input process with thermal storage, Applied Energy, Volume 160, Pages 308-320, ISSN 0306-2619

[19] ANSI/AHRI Standard 540, 2004. "Standard for Performance Rating of Positive Displacement Refrigerant Compressors and Compressor Units"

[20] R. Soltani and M. R. I. Dincer, "Comparative performance evaluation of cascaded air-source hydronic heat pumps," *Energy Conversion and Management,* no. 89, pp. 577-587, 2015.

[21] Dabiri, A.E., Rice, C.K., 1981. "A compressor simulation model with corrections for the level of suction gas superheat," ASHRAE Transactions 87 (2), 771–780.

[22] M. J. Moran, H. N. Shapiro, D. D. Boettner and M. B. Bailey, "Fundamentals of Engineering Thermodynamics 7ed," Hoboken: John Wiley & Sons, 2010.

[23] Goswani, D.Y., F. Kreith, and J.F. Kreider, Principles of Solar Engineering, 2nd Edition, Taylor and Frances, 2003.

[24] Markvart, T. (2003). Practical handbook of photovoltaics: Fundamentals and applications. New York: Elsevier Advanced Technology.

[25] G. Bellenda, "Powertherm Thermal Test Report, Test Report Number M1.11.NRG.0319/43724," Torino, 2011.

[26] NSRDB: 1991- 2005 Update: TMY3. Retrieved February 14, 2016, from http://rredc.nrel.gov/solar/old_data/nsrdb/1991-2005/tmy3/

[27] Engineering Climate Datasets. Retrieved February 14, 2016, from http://climate.weather.gc.ca/prods_servs/engineering_e.html

[28] Solar Rating and Certification Corporation, "Solar Panels Plus SPP-30 Thermal Performace Rating," Cocoa, 2009.

[29] The RETScreen Clean Energy Project Analysis Software 4.0, Natural Resources Canada–Canmet ENERGY

[30] Emerson Climate Technologies. (2010). ZB15KQE-PFJ Ratings Coefficients

[31] Lemmon, E.W., Huber, M.L., McLinden, M.O. NIST Standard Reference Database 23: Reference Fluid Thermodynamic and Transport Properties-REFPROP, Version 9.1, National Institute of Standards and Technology, Standard Reference Data Program, Gaithersburg, 2013.

[32] Emerson Climate Technologies. (2010). ZB15KQE-PFJ Ratings Coefficients

[33] Lemmon, E.W., Huber, M.L., McLinden, M.O. NIST Standard Reference Database 23: Reference Fluid Thermodynamic and Transport Properties-REFPROP, Version 9.1, National Institute of Standards and Technology, Standard Reference Data Program, Gaithersburg, 2013.
[34] Guangzhou Qilin Environmental Technology Firm. (2016). Copleand Scroll Compressor Price. Retrieved from http://www.alibaba.com/product-detail/Copleand-Scroll-Compressor-ZB15KQE-PFJ-558_1118991563.html
[35] POKKA Automotive air conditioning parts export co., LTD. (2016). Air Conditioner Expension Valve Price. Retrieved from http://www.aliexpress.com/item/Free-Shipping-Fujikoki-Thailand-Expansion-valve-9-16-OR-3-8-OR-Air-conditioner-expansion-valve/32647847244.html?spm
[36] McMaster-Carr. (2016). Heat Exchanger Price. Retrieved from http://www.mcmaster.com/#35115k61/=135z2ja
[37] The World's Trusted Currency Authority. (n.d.). Retrieved July 07, 2016, from http://www.xe.com/currencyconverter/convert/?Amount=1
[38] Natural Resources Canada. (2012). Water heater guide. Ottawa.
[39] Ontario Energy Board. (2016, June 23). Natural Gas Rate Updates. Retrieved July 8, 2016, from http://www.ontarioenergyboard.ca/OEB/Consumers/Natural Gas/Natural Gas Rates
[40] EPCOR. (2016). Historical Natural Gas Rates. Retrieved July 08, 2016, from http://www.epcor.com/power-natural-gas/energy-plans/energy-plans/Pages/historical-natural-gas-rates.aspx
[41] U.S. Energy Information Administration - EIA - Independent Statistics and Analysis. (2016). Retrieved July 08, 2016, from https://www.eia.gov/naturalgas/
[42] Solimpeks Solar Energy Corp. (2012). Volther PowerTherm & PowerVolt Datasheet [Brochure]. Konya: Author.